# Supplemental Material for "Optimal face-to-face coupling for fast self-folding kirigami"

Maks Pecnik Bambic,[a,b,c] Nuno A. M. Araújo,[d,e] and Benjamin J. Walker,[f,g] Duncan R. Hewitt,[g] Qing Xiang Pei,[b] Ran Ni,[c] Giorgio Volpe[a*]

[a] Department of Chemistry, University College London, 20 Gordon Street, WC1H 0AJ London, United Kingdom
[b] Institute of High Performance Computing, A*STAR, Singapore
[c] School of Chemistry, Chemical Engineering and Biotechnology, Nanyang Technological University, 62 Nanyang Drive, 637459, Singapore
[d] Departamento de Física, Faculdade de Ciências, Universidade de Lisboa, 1749-016 Lisboa, Portugal
[e] Centro de Física Teórica e Computacional, Faculdade de Ciências, Universidade de Lisboa, 1749-016 Lisboa, Portugal
[f] Department of Mathematical Sciences, University of Bath, Claverton Down, Bath, BA2 7AY, United Kingdom
[g] Department of Mathematics, University College London, Gordon Street, London, WC1H 0AY, United Kingdom

## Hydrodynamic coupling in the overdamped motion of two hinged sheets

Here, we formulate a relatively simple mechanical model for the motion of two flat sheets that are connected by a hinge, evolving in an ambient fluid on such a scale that inertial effects are negligible. Seeking a first-order approximation and analytical tractability, we make use of *resistive force theory* [1,2] to couple the object's motion to the fluid. This approach neglects secondary hydrodynamic interactions between the sheets and assigns constant drag coefficients to each sheet.

We focus on the two-dimensional motion of the sheets in a plane orthogonal to both, thus constraining their motion as shown in Fig. 1. In this set up, the two flat sheets are assumed to extend out of the plane of the figure. For simplicity, we consider identical sheets of equal length, $h$, here, although we quote more general results for sheets of different length below. Pinning the end of the lower sheet to a substrate ($s=0$), the configuration of the connected object in this setting is captured by the orientation $\theta_\mathrm{l}$ of the lower sheet and the orientation $\varphi$ of the upper sheet, both measured relative to an axis fixed in the laboratory frame. We will first formulate the model in terms of $\theta_\mathrm{l}$ and $\varphi$ and later rewrite it in terms of $\theta_\mathrm{l}$ and $\theta_\mathrm{u} \coloneqq \varphi - \theta_\mathrm{l}$, the relative angle between the sheets. Noting that each sheet is assumed to be flat, we define the tangents $\boldsymbol{t}_\mathrm{l}$ and $\boldsymbol{t}_\mathrm{u}$ and normals $\boldsymbol{n}_\mathrm{l}$ and $\boldsymbol{n}_\mathrm{u}$ to each sheet, given respectively by

$$\boldsymbol{t}_\mathrm{l} = \cos\theta_\mathrm{l}\boldsymbol{e}_x + \sin\theta_\mathrm{l}\boldsymbol{e}_y\,, \qquad \boldsymbol{n}_\mathrm{l} = -\sin\theta_\mathrm{l}\boldsymbol{e}_x + \cos\theta_\mathrm{l}\boldsymbol{e}_y\,, \tag{1a}$$

$$\boldsymbol{t}_\mathrm{u} = \cos\varphi\boldsymbol{e}_x + \sin\varphi\boldsymbol{e}_y\,, \qquad \boldsymbol{n}_\mathrm{u} = -\sin\varphi\boldsymbol{e}_x + \cos\varphi\boldsymbol{e}_y\,, \tag{1b}$$

where $\boldsymbol{e}_x$ and $\boldsymbol{e}_y$ form part of the right-handed orthonormal basis $\{\boldsymbol{e}_x, \boldsymbol{e}_y, \boldsymbol{e}_z\}$ of the laboratory frame (Fig. 1). With this notation, we can write the position $\boldsymbol{x}(s)$ of a material point in the plane as

$$\boldsymbol{x}(s) = \begin{cases} s\boldsymbol{t}_\mathrm{l} & \text{if } s\in[0,h)\,, \\ h\boldsymbol{t}_\mathrm{l} + (s-h)\boldsymbol{t}_\mathrm{u} & \text{if } s\in[h,2h]\,, \end{cases} \tag{2}$$

where $s\in[0,2h]$ is an arclength parameter measured from the pinned end, which we have taken to be the origin of the laboratory frame ($s=0$, Fig. 1). We will relate the forces imparted on each sheet by the fluid to the velocity of the sheets, which we compute as

$$\dot{\boldsymbol{x}}(s) = \begin{cases} s\dot{\theta}_\mathrm{l}\boldsymbol{n}_\mathrm{l} & \text{if } s\in[0,h)\,, \\ h\dot{\theta}_\mathrm{l}\boldsymbol{n}_\mathrm{l} + (s-h)\dot{\varphi}\boldsymbol{n}_\mathrm{u} & \text{if } s\in[h,2h]\,. \end{cases} \tag{3}$$

Employing resistive force theory [1,2], we suppose the existence of tangential and normal resistive force coefficients, $C^t$ and $C^n$, for each sheet such that the force per unit length $\boldsymbol{f}(s)$ exerted on each sheet is given by

$$\boldsymbol{f}(s) = C^t\left[\dot{\boldsymbol{x}}(s)\cdot\boldsymbol{t}(s)\right]\boldsymbol{t}(s) + C^n\left[\dot{\boldsymbol{x}}(s)\cdot\boldsymbol{n}(s)\right]\boldsymbol{n}(s)\,, \tag{4}$$

where $\boldsymbol{t}(s)$ and $\boldsymbol{n}(s)$ denote the tangent and normal associated with arclength $s$, for brevity. Here, $C^t<0$ and $C^n<0$, so that $\boldsymbol{f}$ indeed captures a notion of hydrodynamic drag. Again, we assume for simplicity that each sheet has the same resistive force coefficients; this assumption is also relaxed in the general results quoted below. In fact, the results of our analysis will not depend strongly on the appropriate values of $C^n$ and $C^t$, though we remark that, in the context of thin filaments rather than sheets, the approximate relation $C^n \approx 2C^t$ holds [1,2], with $C^t/C^n < 1$ expected for more general sheet shapes [3].

In the inertialess regime appropriate for the scales involved in this problem, equations of moment balance apply on each sheet.

* Corresponding author: g.volpe@ucl.ac.uk

That is, the moments induced by the hydrodynamic drag must instantaneously balance those induced by any applied forces or torques. These two conditions will uniquely determine $\theta_\mathrm{l}$ and $\varphi$. Here, we will assume that the system is driven by two point forces that act at the connecting hinge and the free end of the upper sheet, denoting the magnitudes of these forces by $F_\mathrm{l}$ and $F_\mathrm{u}$, respectively. Further, we will consider only prescribed forces that drive rotation of the sheets by acting in the normal direction, so that they exert forces $F_\mathrm{l}\boldsymbol{n}_\mathrm{l}$ and $F_\mathrm{u}\boldsymbol{n}_\mathrm{u}$, respectively. We additionally allow for the possibility of a prescribed (though potentially state-dependent) point torque $m\boldsymbol{e}_z$ to act at the connecting hinge.

With these driving terms, it is convenient to write the two constraints of moment balance as two integrals, one over only the upper sheet and another over both sheets, resolving moments about the hinge and the lower end, respectively. Explicitly, we have

$$0 = \boldsymbol{e}_z \cdot \int_h^{2h} [\boldsymbol{x}(s) - \boldsymbol{x}(h)] \times \boldsymbol{f}(s)\, \mathrm{d}s + hF_\mathrm{u} + m\,, \tag{5a}$$

$$0 = \boldsymbol{e}_z \cdot \int_0^{2h} \boldsymbol{x}(s) \times \boldsymbol{f}(s)\, \mathrm{d}s + hF_\mathrm{l} + hF_\mathrm{u}[1 + \cos(\varphi - \theta_\mathrm{l})]\,, \tag{5b}$$

imposing a moment-free condition at the end of the upper sheet. Computing the required integrals along each sheet yields the explicit linear system of equations

$$-\frac{C^n h^2}{6}\begin{bmatrix} 2 & 2+3\cos\theta_\mathrm{u} \\ 2+3\cos\theta_\mathrm{u} & 4+6\cos\theta_\mathrm{u}\,(1+\cos\theta_\mathrm{u}) + 6\frac{C^t}{C^n}\sin^2\theta_\mathrm{u} \end{bmatrix}\begin{bmatrix}\dot\theta_\mathrm{u}\\ \dot\theta_\mathrm{l}\end{bmatrix} = \begin{bmatrix} 1 & 0 & 1 \\ (1+\cos\theta_\mathrm{u}) & 1 & 0\end{bmatrix}\begin{bmatrix} F_\mathrm{u}\\ F_\mathrm{l}\\ m/h\end{bmatrix}, \tag{6}$$

recalling that $\theta_\mathrm{u} = \varphi - \theta_\mathrm{l}$ is the relative angle between the two sheets and that $C^n < 0$. We can manipulate this system by subtracting $(1+\cos\theta_\mathrm{u})$ multiplied by the first equation from the second to simplify the dependence on $F_\mathrm{u}$ and $F_\mathrm{l}$:

$$-\frac{C^n h^2}{6}\begin{bmatrix} 2 & -2\hat\alpha(\theta_\mathrm{u}) \\ \cos\theta_\mathrm{u} & -\cos\theta_\mathrm{u}/\hat\beta(\theta_\mathrm{u})\end{bmatrix}\begin{bmatrix}\dot\theta_\mathrm{u}\\ \dot\theta_\mathrm{l}\end{bmatrix} = \begin{bmatrix} 1 & 0 & 1 \\ 0 & 1 & -(1+\cos\theta_\mathrm{u})\end{bmatrix}\begin{bmatrix} F_\mathrm{u}\\ F_\mathrm{l}\\ m/h\end{bmatrix}, \tag{7}$$

where

$$\hat\alpha(\theta_\mathrm{u}) = -\left[1 + \frac{3}{2}\cos\theta_\mathrm{u}\right], \quad \hat\beta(\theta_\mathrm{u}) = \frac{-\cos\theta_\mathrm{u}}{2+\cos\theta_\mathrm{u}\,(1+3\cos\theta_\mathrm{u}) + 6(C^t/C^n)\sin^2\theta_\mathrm{u}}\,. \tag{8}$$

Equation (7) shows how the angular variables relate to the corresponding forces, and highlights how a particular choice of the active hinge torque $m$ could qualitatively change this relationship (for instance if $m \propto \dot\theta_\mathrm{u}$ or $m \propto \dot\theta_\mathrm{l}$). For simplicity here, we focus on a free hinge with $m = 0$, leading to the results quoted in the main text:

$$\dot\theta_\mathrm{u} = \hat\alpha(\theta_\mathrm{u})\dot\theta_\mathrm{l} - \frac{3}{C^n h^2}F_\mathrm{u}, \tag{9a}$$

$$\dot\theta_\mathrm{l} = \hat\beta(\theta_\mathrm{u})\dot\theta_\mathrm{u} + \frac{6\hat\beta(\theta_\mathrm{u})}{\cos(\theta_\mathrm{u})C^n h^2}F_\mathrm{l}. \tag{9b}$$

For sheets oriented approximately parallel to one another, in particular those with $|\theta_\mathrm{u}| \ll 1$, the functions $\hat\alpha$ and $\hat\beta$ simplify substantially to leading order in powers of $\theta_\mathrm{u}$ to yield the approximate, constant-coefficient system from Eq. (7),

$$2\dot\theta_\mathrm{u} = -5\dot\theta_\mathrm{l} - \frac{6}{C^n h^2}F_\mathrm{u}\,, \tag{10a}$$

$$\dot\theta_\mathrm{u} = -6\dot\theta_\mathrm{l} - \frac{6}{C^n h^2}F_\mathrm{l}\,. \tag{10b}$$

From this, we can see that if one were to drive the system via only the lower sheet, so that $F_\mathrm{u} = 0$ and $F_\mathrm{l} \neq 0$, the reorientation rate of the upper sheet is $\dot\theta_\mathrm{u} \sim -5\dot\theta_\mathrm{l}/2$. Conversely, if one were to drive the system via only the upper sheet, so that $F_\mathrm{l} = 0$ and $F_\mathrm{u} \neq 0$, the reorientation rate of the lower sheet is $\dot\theta_\mathrm{l} \sim -\dot\theta_\mathrm{u}/6$. Hence, in this sense, the coupling between $\theta_\mathrm{u}$ and $\theta_\mathrm{l}$ is dominated by a negative feedback in the motion of the upper sheet. More generally, the application of any driving force of the form considered here has a greater impact on the relative orientation of the upper sheet than it does on the orientation of the lower sheet, at least in the small relative-angle regime. The validity of these conclusions outside this small-angle regime hinges on the relative size of $\hat\alpha$ and $\hat\beta$ in Eq. 9. These are shown for a range of angles in Fig. 2, which illustrates that they differ by approximately an order of magnitude across a large range of $\theta_\mathrm{u}$; this difference confirms that forcing drives larger changes in $\theta_\mathrm{u}$ than in $\theta_\mathrm{l}$ in general.

More generally, it is straightforward, if somewhat involved, to repeat this analysis allowing for different lengths $h_\mathrm{l}$ and $h_\mathrm{u}$ of each sheet, and different resistive force coefficients $C^n_\mathrm{u}$, $C^n_\mathrm{l}$, $C^t_\mathrm{u}$, $C^t_\mathrm{l}$. Omitting the details and no longer assuming $m = 0$, the equivalent

expressions in that case also involve the length ratio $R \equiv h_\mathrm{u}/h_\mathrm{l}$ and the normal resistive force ratio $\Gamma \equiv C^n_\mathrm{u}/C^n_\mathrm{l}$ and are

$$\dot{\theta}_\mathrm{u} = \hat{\alpha}(\theta_\mathrm{u})\dot{\theta}_\mathrm{l} - \frac{3}{C^n_\mathrm{u} h^2_\mathrm{u}}\left(F_\mathrm{u} + \frac{m}{h_\mathrm{u}}\right), \tag{11a}$$

$$\dot{\theta}_\mathrm{l} = \hat{\beta}(\theta_\mathrm{u})\dot{\theta}_\mathrm{u} + \frac{6\hat{\beta}(\theta_\mathrm{u})}{C^n_\mathrm{u} h^2_\mathrm{u}(3-2R)\cos\theta_\mathrm{u}}\left[F_\mathrm{l} - R(1+\cos\theta_\mathrm{u})\frac{m}{h_\mathrm{u}}\right], \tag{11b}$$

with

$$\hat{\alpha}(\theta_\mathrm{u}) = -\left[1 + \frac{3}{2R}\cos\theta_\mathrm{u}\right], \quad \hat{\beta}(\theta_\mathrm{u}) = \frac{(3-2R)\cos\theta_\mathrm{u}}{2/(\Gamma R^2) + \cos\theta_\mathrm{u}\,[3-2R+(6/R-3)\cos\theta_\mathrm{u}] + 6[C^t_\mathrm{u}/(C^n_\mathrm{u}R)]\sin^2\theta_\mathrm{u}}. \tag{12}$$

These expressions illustrate how the strength of coupling between the sheets can be modified by suitable choice of the ratios $R$ and $\Gamma$, as well as by the active hinge torque $m$ if it has some dependence on $\dot{\theta}_\mathrm{u}$ or $\dot{\theta}_\mathrm{l}$.

## Deriving a diffusion coefficient

We derive an approximate rotational diffusion coefficient for each face of the kirigami, assuming that faces are entirely uncoupled. Let us consider a face in a fluid at thermostat temperature $T$, connected by a hinge to a surface such that it can only rotate around one edge. If this edge is a principle axis of inertia, the equation of motion for the angle $\theta(t)$ with the surface is,

$$I\ddot{\theta}(t) = -f_\mathrm{r}\dot{\theta}(t) + \Xi\xi(t), \tag{13}$$

where $t$ is time, $I$ is the corresponding momentum of inertia, $f_\mathrm{r}$ is the frictional resistance coefficient, $\xi(t)$ is a stochastic term with zero mean and variance one, and $\Xi$ sets the amplitude of the thermal fluctuations in the force. Thus, for $\theta(0) \equiv 0$, the mean-square displacement of the angle $\theta(t)$ is,

$$\langle\theta^2(t)\rangle \sim \left[\frac{\Xi^2}{If_\mathrm{r}^2}\right]t. \tag{14}$$

The dependence of $\Xi$ on $T$ and $f_r$ can be derived by invoking equipartion as follows. The equation for the angular velocity $\omega \equiv \dot{\theta}$ is

$$I\dot{\omega}(t) = -f_\mathrm{r}\omega(t) + \Xi\xi(t). \tag{15}$$

Assuming the same initial velocity $\omega(0) \equiv \omega_0$, the mean-square velocity is then,

$$\langle\omega^2(t)\rangle = \omega_0^2\exp\left(-\frac{2f_\mathrm{r}}{I}t\right) + \frac{\Xi^2}{2If_\mathrm{r}}\left[1-\exp\left(-\frac{2f_\mathrm{r}}{I}t\right)\right]. \tag{16}$$

Asymptotically, from the equipartition theorem, $\omega^2 = k_\mathrm{B}T/I$, where $k_\mathrm{B}$ is the Boltzmann constant, and thus,

$$\Xi = \sqrt{2f_\mathrm{r}k_\mathrm{B}T}\ . \tag{17}$$

Combining with Eq. (14), we obtain the Einstein relation,

$$D = \frac{k_\mathrm{B}T}{f_\mathrm{r}}\ . \tag{18}$$

The frictional resistance coefficient $f_\mathrm{r}$ of the plate is computed as the ratio of applied torque and the resulting angular velocity. Computing this ratio is in fact a subproblem of the above section, exactly equivalent to considering the torque balance on only the bottom face. This immediately yields

$$f_\mathrm{r} = -\frac{C^n h^3}{3} \tag{19}$$

for normal resistive coefficient $C^n$. In the absence of an exact expression for $C^n$ for a general plate, we approximate the face as a circular disc of radius $h/\sqrt{\pi}$. A circular disc with this radius that moves at unit speed normal to its radii in a medium of viscosity $\mu$ experiences total drag $16\mu h/\sqrt{\pi}$[4]. Crudely dividing this quantity by its diameter to yield a representative drag per unit length gives a drag coefficient of $C^n = -8\mu$. Hence, we approximate

$$f_\mathrm{r} \approx \frac{8\mu h^3}{3}. \tag{20}$$

Finally, the Einstein relation gives

$$D = \frac{k_\mathrm{B}T}{f_\mathrm{r}} = \frac{3k_\mathrm{B}T}{8\mu h^3} \tag{21}$$

as an estimate for the rotational diffusion coefficient of a single face.

In our simulations, the rotational diffusion coefficient was fixed to $D = 0.64$ rad$^2$ s$^{-1}$. Figure 3 shows that, qualitatively, the dependence (i.e. the position of the peak) of the normalized folding rate $k_\alpha/k_0$ ($k_0$ being $k_\alpha$ for $\alpha = 0$) on $\alpha$ is largely independent of the exact value of the diffusion coefficient for structures whose face height $h$ is on the scale of $\mathscr{O}(\mu\text{m})$ to $\mathscr{O}(10\,\mu\text{m})$. At larger scales (i.e. by increasing $h$ further), gravitational torques will also need to be accounted for to determine the overall folding behavior[5].

## Mapping to a first passage time problem

For pyramids with less than five faces, it has been shown that the folding time is dominated by the time it takes for the first pair of faces to close[6,7]. Equally, for two-level structures, if we assume that the lower level folds much faster than the upper one, the folding time can be estimated as the time it takes for the first pair of faces of the upper level to meet at their target angle $\phi_\text{u}$, after the lower level has closed completely. The time evolution of the angles of these two faces can be mapped into a two-dimensional Brownian walk (one dimension for each face) and we can neglect collisions between faces, as suggested by molecular dynamics simulations in Ref.[7]. If we discretize the configuration space, the motion of the faces corresponds to a random walk on a lattice with $L$ points per dimension with reflective boundaries. In the most general case, such a two-dimensional lattice is bound at $-\pi$ and $\pi$ along each direction and spaced every $\Delta = \pi/180$. Finding the closing time of a pair of faces corresponds to determining the first-passage time for the two-dimensional random walk visiting the lattice site $\boldsymbol{\phi} = (\phi_\text{u}, \phi_\text{u})$, equivalent to both faces reaching $\phi_\text{u}$ at the same time. The walk begins at $\boldsymbol{\theta}_0 = (\theta_{01}, \theta_{02})$, the subscripts 1 and 2 referring to each of the two faces respectively. The Mean First Passage Time (MFPT) for such a walk can be obtained through[8]

$$T_{\boldsymbol{\theta}_0 \to \boldsymbol{\phi}} = 8\left[\sum_{\theta_1=1,\theta_2=1}^{L-1} K_{\theta_1,\theta_2}(\boldsymbol{\theta}_0,\boldsymbol{\phi}) + \frac{1}{2}\sum_{\theta_1=1}^{L-1} K_{\theta_1,0}(\boldsymbol{\theta}_0,\boldsymbol{\phi}) + \frac{1}{2}\sum_{\theta_2=1}^{L-1} K_{0,\theta_2}(\boldsymbol{\theta}_0,\boldsymbol{\phi})\right], \tag{22}$$

where $\boldsymbol{\theta} = (\theta_1, \theta_2)$ represents a generic lattice position, and

$$\begin{aligned} K_{\theta_1,\theta_2}(\boldsymbol{\theta}_0,\boldsymbol{\phi}) = \Bigg[&\cos^2\left[\left(\phi_\text{u}+\frac{1}{2}\right)\frac{\theta_1\pi}{L}\right]\cos^2\left[\left(\phi_\text{u}+\frac{1}{2}\right)\frac{\theta_2\pi}{L}\right] - \cos\left[\left(\theta_1+\frac{1}{2}\right)\frac{\theta_1\pi}{L}\right]\cos\left[\left(\theta_2+\frac{1}{2}\right)\frac{\theta_2\pi}{L}\right]\times \\ &\times\cos\left[\left(\phi_\text{u}+\frac{1}{2}\right)\frac{\theta_1\pi}{L}\right]\cos\left[\left(\phi_\text{u}+\frac{1}{2}\right)\frac{\theta_2\pi}{L}\right]\Bigg]\times\left[2-\cos\left(\frac{\theta_1\pi}{L}\right)-\cos\left(\frac{\theta_2\pi}{L}\right)\right]^{-1}. \end{aligned} \tag{23}$$

Equation (22) represents the MFPT while Eq. (23) is the lattice propagator function for a two-dimensional random walk in a bounded domain[8]. A summation over the whole discretized space is therefore considered in order to establish the possible evolutions of the two-dimensional walk starting at $\boldsymbol{\theta}_0$ and ending at $\boldsymbol{\phi}$.

If we assume that the motion of the different faces in the upper level is uncorrelated and that the probability distribution of the angles $\mathscr{N}(\mu,\sigma)$ is a Gaussian reflected at the lattice boundaries, the probability of starting at a given lattice position can be calculated as

$$P(\boldsymbol{\theta}_0) = \mathscr{N}(\mu,\sigma)_{|\theta_{01}}\mathscr{N}(\mu,\sigma)_{|\theta_{02}}\,. \tag{24}$$

We can thus obtain an expected MFPT, $\langle\tau_\text{f}(\mu)\rangle$, by first calculating $T_{\boldsymbol{\theta}_0\to\boldsymbol{\phi}}$ for every lattice position, multiplying it by the probability $P(\boldsymbol{\theta}_0)$ of starting at that point and integrating over the whole range of possible starting positions $\boldsymbol{\theta}_0$

$$\langle\tau_\text{f}(\mu)\rangle = \iint T_{\boldsymbol{\theta}_0\to\boldsymbol{\phi}} P(\boldsymbol{\theta}_0)\, d\boldsymbol{\theta}_0\,. \tag{25}$$

## Supplemental figures

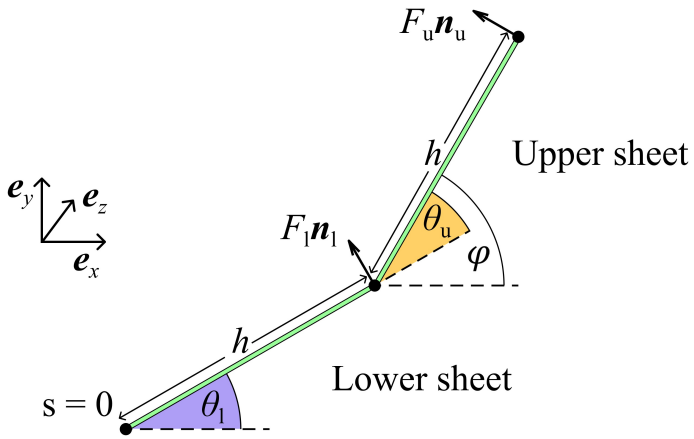


Fig. 1 Model parameterization. Each set of the kirigami's lateral faces (Fig. 1) can be modeled as two flat sheets connected by a hinge with the lower sheet tethered to the substrate ($s = 0$). In the schematics, the sheets are assumed to extend in and out of the plane of the diagram, with all motion occurring within the plane. The configuration of the connected object is captured by the orientation $\theta_l$ of the lower sheet and $\varphi$ of the upper sheet (both defined in the laboratory frame, $\{\boldsymbol{e}_x, \boldsymbol{e}_y, \boldsymbol{e}_z\}$). Alternatively, the orientation of the upper sheet can be captured by $\theta_u := \varphi - \theta_l$. The object is driven by two point forces, $F_l$ and $F_u$, acting respectively on the lower and upper hinges and directed along the normals to each sheet ($\boldsymbol{n}_l$ and $\boldsymbol{n}_u$).

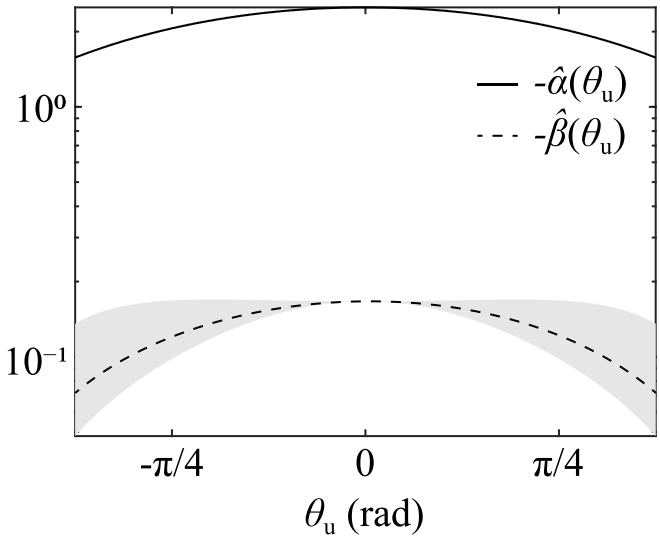


Fig. 2 Relative coupling between $\theta_u$ and $\theta_l$ as a function of $\theta_u$. Functions $-\hat{\alpha}(\theta_u)$ (solid) and $-\hat{\beta}(\theta_u)$ (dashed) on a logarithmic scale for a range of $\theta_u$, for the case of equal sheet lengths and equal resistive force components, highlighting the order-of-magnitude dominance of the former over the latter. Recall that these represent the negative feedback of motion of the lower face on the upper and motion of the upper on the lower, respectively (see eq. (9)). The lines have $C^t/C^n = 1/2$, appropriate for slender filaments; the shaded region shows the range of possible values for $0 \leq C^t/C^n \leq 1$, illustrating that the qualitative result is largely insensitive to this ratio.

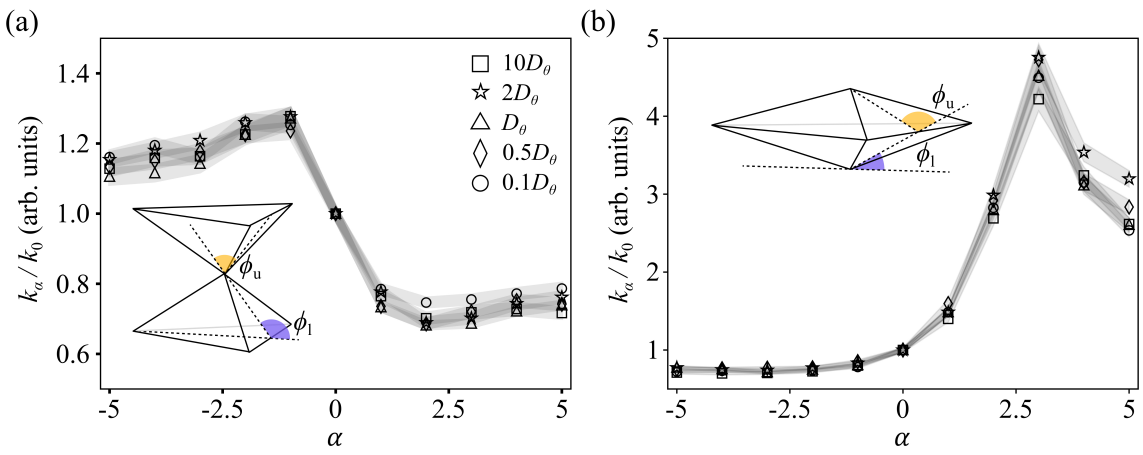


Fig. 3 Dependence of the normalized folding rate on the rotational diffusion coefficient. Normalized folding rate $k_\alpha/k_0$ as a function of coupling parameter $\alpha$ for two exemplary kirigami structures (as in Fig. 2) with different rotational diffusion coefficients: (a) a hourglass ($\phi_l = \frac{\pi}{3}$ rad, $\phi_u = -\frac{\pi}{6}$ rad) and (b) a diamond ($\phi_l = 0.61$ rad, $\phi_u = 1.92$ rad). Folding rates are normalized to $k_0$ ($k_\alpha$ for $\alpha = 0$). The shaded areas represent one standard error around the average values from 5000 folding events per value of rotational diffusion constant, each lasting up to the cutoff time $\tau_{cut} = 2 \cdot 10^8 \Delta\tau$ (with $\Delta\tau$ being the simulation time step).

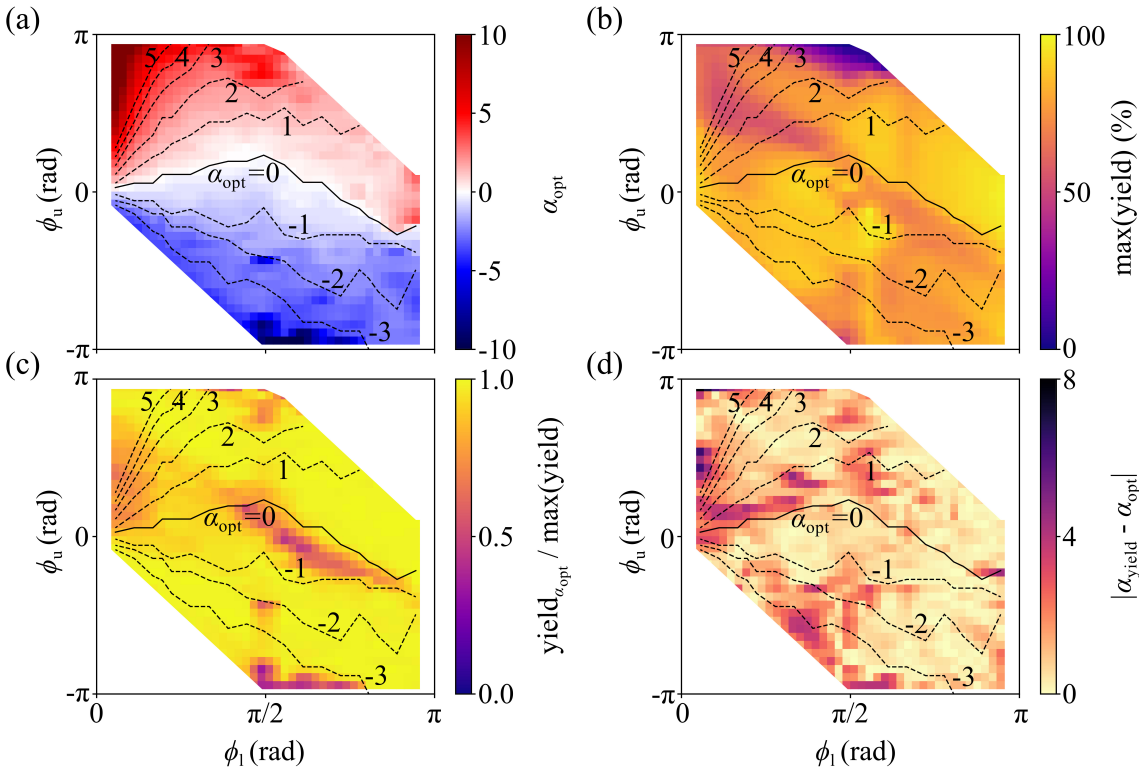


Fig. 4 Optimal rate vs. optimal yield. (a) Optimal $\alpha$ value ($\alpha_{opt}$) leading to the highest folding rate $\max(k_\alpha)$, (b) highest folding yield $\max(\text{yield})$ at any $\alpha$, (c) ratio between yield at $\alpha_{opt}$ ($\text{yield}_{\alpha_{opt}}$) and $\max(\text{yield})$ at any value of $\alpha$, (d) distance between $\alpha$ values that optimizes yield ($\alpha_{yield}$) and $\alpha_{opt}$ for different target structures. In (a-d), the black dashed isolines show the optimal values of $\alpha$ that lead to the highest folding rates and the black solid lines highlight structures whose folding is optimal in the absence of coupling ($\alpha = 0$) for reference. Each data point is obtained as an average of 5000 folding events.

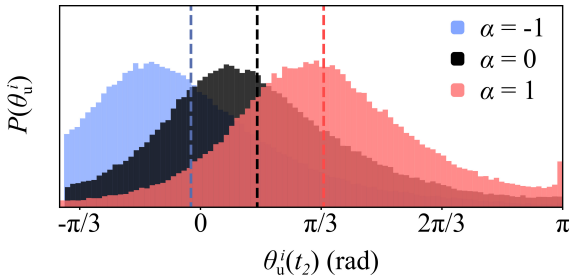


Fig. 5 Probability distributions of the upper level's faces at the closing time of the lower level. Examples of probability distributions $P(\theta_u^i)$ of the angles $\theta_u^i$ of the upper level's faces at the closing time of the lower level $t_2$ for the structure of Fig. 1 for $\alpha = -1$, $\alpha = 0$ and $\alpha = 1$. The vertical dashed lines represent the means $\mu(\alpha) = \langle \theta_u^i(t_2) \rangle_\alpha$ of the same-color distributions. Each distribution is obtained from 50000 structures.

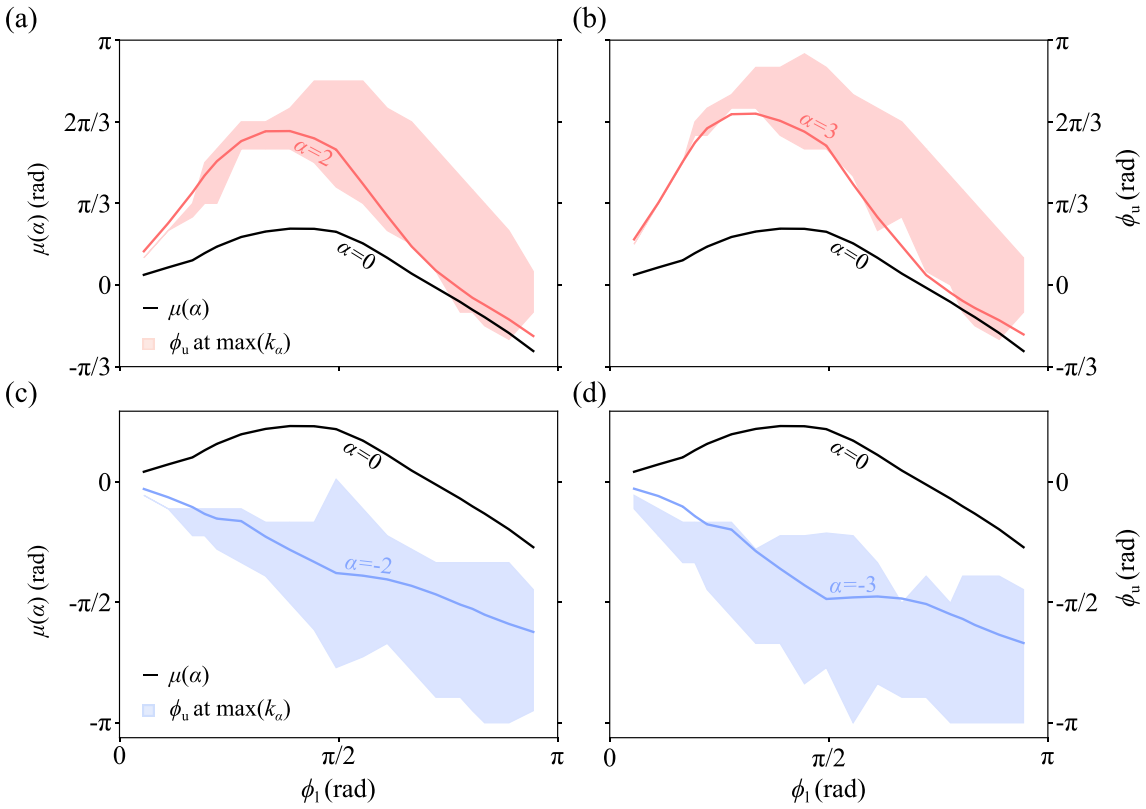


Fig. 6 Target geometry and optimal $\alpha$. For a given $\alpha$, the means $\mu(\alpha) = \langle \theta_u^i(t_2) \rangle_\alpha$ (solid lines) of the probability distributions of the angles $\theta_u^i$ of the upper level's faces at the closing time $t_2$ of the lower level are well reproduced by the structures (represented as combinations of the two target angles $\phi_u$ and $\phi_l$) with the highest folding rate at that value of $\alpha$ (shaded regions): (a) $\alpha = 2$, (b) $\alpha = 3$, (c) $\alpha = -2$ and (d) $\alpha = -3$. The black solid lines show $\mu(\alpha = 0)$ for reference. The shaded regions represent all structures that could have the highest folding rate at that value of $\alpha$ once the numerical uncertainty is accounted for. For a given structure, this uncertainty around the position of $\max(k_\alpha)$ is calculated taking the largest between the discretization step in $\alpha$ and the range of data points around the peak falling within the standard error.

## Notes and references


1 G. J. Hancock, *Proc. Math. Phys. Eng. Sci.*, 1953, **217**, 96–121.

2 J. Gray and G. J. Hancock, *J. Exp. Biol.*, 1955, **32**, 802–814.

3 L. Koens and E. Lauga, *Phys. Fluids*, 2016, **28**, 013101.

4 A. M. Davis, *J. Fluid Mech.*, 1991, **231**, 51–71.

5 T. G. Leong, P. A. Lester, T. L. Koh, E. K. Call and D. H. Gracias, *Langmuir*, 2007, **23**, 8747–8751.

6 T. S. A. N. Simões, H. P. M. Melo and N. A. M. Araújo, *Eur. Phys. J. E. Soft Matter*, 2021, **44**, 46–46.

7 H. Melo, C. Dias and N. Araújo, *Commun. Phys.*, 2020, **3**, 154.

8 L. Giuggioli, *Phys. Rev. X*, 2020, **10**, 021045.